

Article

Shock Properties Characterization of Dielectric Materials Using Millimeter-Wave Interferometry and Convolutional Neural Networks

Jérémi Mapas ¹, Alexandre Lefrançois ^{1,*}, Hervé Aubert ², Sacha Comte ¹, Yohan Barbarin ¹ ,
Maylis Lavayssière ¹ , Benoit Rougier ¹ and Alexandre Dore ²

¹ CEA-DAM, GRAMAT, BP80200, F-46500 Gramat, France

² CNRS-LAAS, Toulouse University, 7 Avenue du Colonel Roche, BP54200, F-31031 Toulouse, France;
aubert@laas.fr (H.A.)

* Correspondence: alexandre.lefrancois@cea.fr

Abstract: In this paper, a neural network approach is applied for solving an electromagnetic inverse problem involving solid dielectric materials subjected to shock impacts and interrogated by a millimeter-wave interferometer. Under mechanical impact, a shock wave is generated in the material and modifies the refractive index. It was recently demonstrated that the shock wavefront velocity and the particle velocity as well as the modified index in a shocked material can be remotely derived from measuring two characteristic Doppler frequencies in the waveform delivered by a millimeter-wave interferometer. We show here that a more accurate estimation of the shock wavefront and particle velocities can be obtained from training an appropriate convolutional neural network, especially in the important case of short-duration waveforms of few microseconds.

Keywords: convolutional neural network; shock properties; mm-wave interferometry; metrology; shock velocity; particle velocity; shock permittivity; shock refractive index



Citation: Mapas, J.; Lefrançois, A.; Aubert, H.; Comte, S.; Barbarin, Y.; Lavayssière, M.; Rougier, B.; Dore, A. Shock Properties Characterization of Dielectric Materials Using Millimeter-Wave Interferometry and Convolutional Neural Networks. *Sensors* **2023**, *23*, 4835. <https://doi.org/10.3390/s23104835>

Academic Editor: Han Haitjema

Received: 9 March 2023

Revised: 4 May 2023

Accepted: 11 May 2023

Published: 17 May 2023



Copyright: © 2023 by the authors. Licensee MDPI, Basel, Switzerland. This article is an open access article distributed under the terms and conditions of the Creative Commons Attribution (CC BY) license (<https://creativecommons.org/licenses/by/4.0/>).

1. Introduction

The physical understanding and modelling of the shock wave propagation in solids has many applications in defense, aeronautics, space and civil areas. In order to simulate the behavior of solids subjected to an impact, it is mandatory to know the mechanical and thermodynamic properties of the pristine and shocked materials. According to the well-documented theory (see, e.g., [1]), the shock wave in dielectric material acts as a moving dielectric interface (or boundary) that propagates faster than the sound in the shocked solid. In the region behind this interface, called the shocked medium, the wave modifies the refractive index of the solid at rest. Moreover, the mechanical impact gives motion to the material, and consequently, it creates a discontinuity in the velocity profile. The velocity of the shocked medium is called the particle velocity, and the fundamental relationship between the shock wavefront velocity V_1 and the particle velocity V_2 is called the shock polar of the material, which can be approximated as follows [2]:

$$V_1 = C_0 + s \cdot V_2 \quad (1)$$

where C_0 ($\text{m} \cdot \text{s}^{-1}$) denotes the speed of sound in the pristine medium at the reference state (i.e., in the solid at rest) and s is a dimensionless constant. The determination of C_0 and s has been the subject of many studies (see, e.g., [2]) and is usually performed from the measurement of V_1 and V_2 [3,4] by using research guns with light gas or powder [5], laser shock [6] or explosives set-ups [7]. Non-invasive techniques were reported to remotely and simultaneously derive the shock wave velocity V_1 , the particle velocity V_2 and possibly the refractive index N_2 of the shocked medium from the measurement of two Doppler frequencies in the waveform delivered by a radiofrequency interferometer [8–13]. The

Doppler effect is a phenomenon where the perceived frequency of sound, light waves or electromagnetic waves changes depending on the relative motion of the source and observer. The impact of the projectile on the material target induces a shock wave. The shock induces a discontinuity change of the material thermodynamic properties before and after the shock front (pressure, velocity, temperature and density). When the interrogation electromagnetic wave passes through the test material, it encounters a moving interface, the shock wave, which is reflective because of the difference in refractive index on either side of the shock wave. The electromagnetic wave is also reflected at the back face of the target, which moves at the speed V_2 . These two reflections induce two frequency Doppler shifts in the final signal corresponding, respectively, to V_1 and V_2 . Therefore, the Doppler effect is coupled on the amplitude and phase of the interrogation radiofrequency signal and is related to the moving interfaces, and consequently, to the velocities V_1 and V_2 . The method in [8] consists of detecting the two Doppler frequencies in the waveform by a fitting process using the linear combination of two sine functions. This radio science paper [8] demonstrates Equations (35)–(37) of this reference. The main conclusion is that there is an analytical solution given by these equations with the three following hypotheses of the physical model: shock velocity V_1 and particle velocity V_2 constant and no dielectric loss. Figure 1 shows a symmetrical impact configuration to study shock properties. The Teflon dielectric waveguide has a variable length ranging from 2 m to 5 m according to the needs, and is used for guiding the millimeter waves to the dielectric sample under shock. The 16 mm in diameter and 80 mm long Teflon cone is glued at the back side of the target to ensure the transition between the dielectric waveguide and the dielectric sample surface. The dielectric cone transition allows the delivery of the millimeter wave generated by the interferometer into the sample during a mechanical impact and to collect the electromagnetic waves reflected by the shocked medium and the surface of the metallic impactor. The impactor is propelled by the Pyrene gas gun and creates a shock at the front surface of the sample, opposite to the dielectric cone interface. The shock physic experiments are plane impact with very limited tilt, less than 5 mrad, performed generally with a light gas gun or a powder gun. So, we analyze the signal in 1D plane configuration without 2D effects from the side release waves. The sustained shock duration is less than 5 μ s. The reflectivity of the shock front is about 2% of the input signal, then if the shock front is too low, the detection of the reflected signal could be an issue, depending on the device sensitivity. The noise could be reduced by choosing the lowest oscilloscope caliber in order to avoid signal saturation. We have observed that, for waveforms of sufficiently long duration ($>5 \mu$ s), the detection and accurate estimation of two Doppler frequencies from the two sinus functions' fitting technique are possible (see, e.g., [9,10] for the investigation of shocked PolyMethylMetAcrylate dielectrics and TriAminoTrinitroBenzene solids, respectively). However, as the waveform duration decreases and is only of a few microseconds, even less than the pulsation period, lower Doppler frequencies may not be accurately estimated, and consequently, the wavefront and particle velocities V_1 and V_2 cannot be derived from the fitting technique reported in [8]. Short-duration waveforms occur in many circumstances, for instance, when the waveform to be processed is less than a time period long due to dielectric losses. Therefore, it is crucial to significantly extend the applicability of millimeter-wave interferometry to the analysis of very short-duration waveforms of a few microseconds. An Artificial Neural Network technique is proposed in this paper to derive V_1 , V_2 and the refractive index N_2 as output neurons of shocked media from time-domain samples of waveforms as input neurons delivered by a millimeter-wave interferometer. The source frequency of the radio-interferometer is 94 GHz, and the wavelength is 3.2 mm. The sample rate is 1 Gsamples/s, and the signal duration is generally a few microseconds. The interrogation distance is between a few millimeters to a hundred millimeters in the target material. Low noise electronic components, especially the IQ mixer, are used to build the radiofrequency interferometer in order to ensure better accuracy. The accuracy on the shock physic velocities depends on the uncertainty of the dielectric properties of the material.

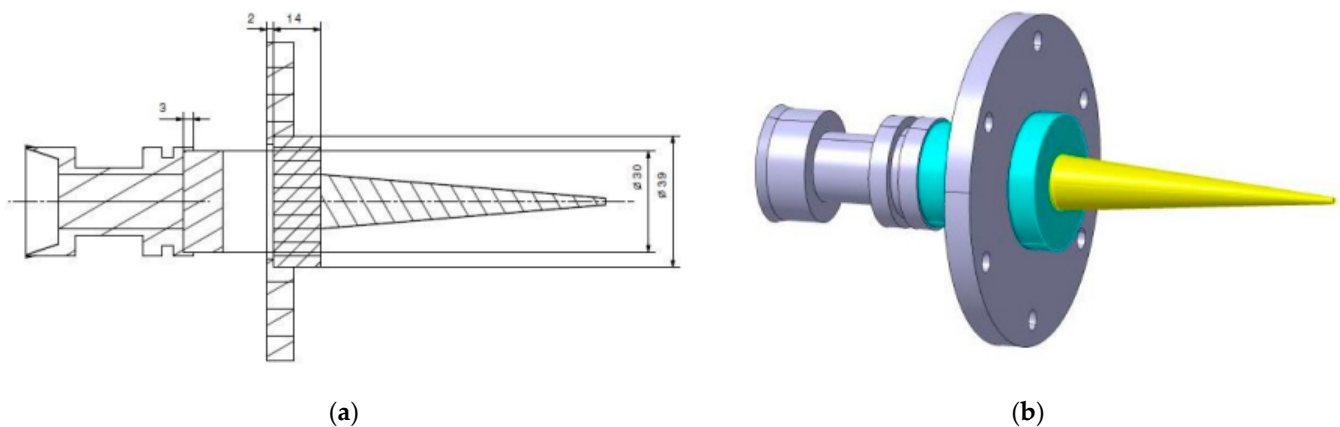


Figure 1. (a) Detail of an impact experimental setup to estimate the shock wavefront and particle velocities in dielectric materials using a 94 GHz interferometer (from left to right: projectile, impactor, target support, target and Teflon cone wave guide end), and (b) 3D view of a symmetrical impact with the same material as impactor and target in light blue (Teflon cone in yellow).

Fully dense Neural Network (NN) models were applied in [14–17] to extract frequencies of interest from some waveforms, but these models are not suitable here. As they require a fixed number of input neurons, these models cannot process waveforms with a variable number of samples. An alternative NN technique consists of using Convolutional Neural Network (CNN) models (see, e.g., [18,19]). CNNs have been widely used in the field of speech recognition, acoustic analysis for leakage, and electrocardiogram analysis for long duration signals of more than one millisecond. The first approach is to use Fast Fourier Transform (FFT), when the frequency is constant, and/or the wavelet method, if the frequency varies. CNN is generally applied for spectrograms to identify complex features and noisy environments are taken into account. The large possible variations in the image or speech recognition and 2D or 1D signals are overcome by the architecture of CNN, thanks to the easier process of weight configurations during training and thanks to local correlations, in order to extract local features [20].

However, in the case of short signals obtained by ultrafast sensors (less than 10 μs), there is no conclusive scientific literature on the use of CNNs. In the case of characterizing the dielectric properties of energetic materials, there is no previous work including the use of CNNs.

The raw signal that we would like to analyze has two frequencies, but they are sustained only during less than a time period. The classical frequential analyses (Fourier Transform, wavelet, etc.) are inaccurate in this case, because there are not enough time periods to give a conclusive result.

We show in this paper that the accurate estimation of velocity V_1 of the shock wavefront, the particle velocity V_2 and the refractive index N_2 of the shocked medium can be estimated from a dedicated CNN, especially for waveforms less than a pulsation period. Indeed, only the first two microseconds are analyzed from the typical waveform, presented in Figure 2. The shock time arrival is near 230.8 μs , when the raw signal oscillation starts. The signal is analyzed from 230.8 μs to 233.5 μs . Between 233.5 μs and 239 μs , the variations of the peak-to-peak signal amplitude are associated with the dielectric loss of the material. After 239 μs , the shock wave enters in the Teflon cone. The high frequency disappears because the shock wave pressure is too low. The period $1/f_1$ is associated with high frequency, around 10 periods between the shock arrival (230.8 μs) and 233.5 μs . The period $1/f_2$ is associated with the low frequency, first period between the shock arrival (230.8 μs) and 233.5 μs . The sample is glued on a metallic transfer plate, which is why, in this case, the radiofrequency interferometer does not show the impactor reflection.

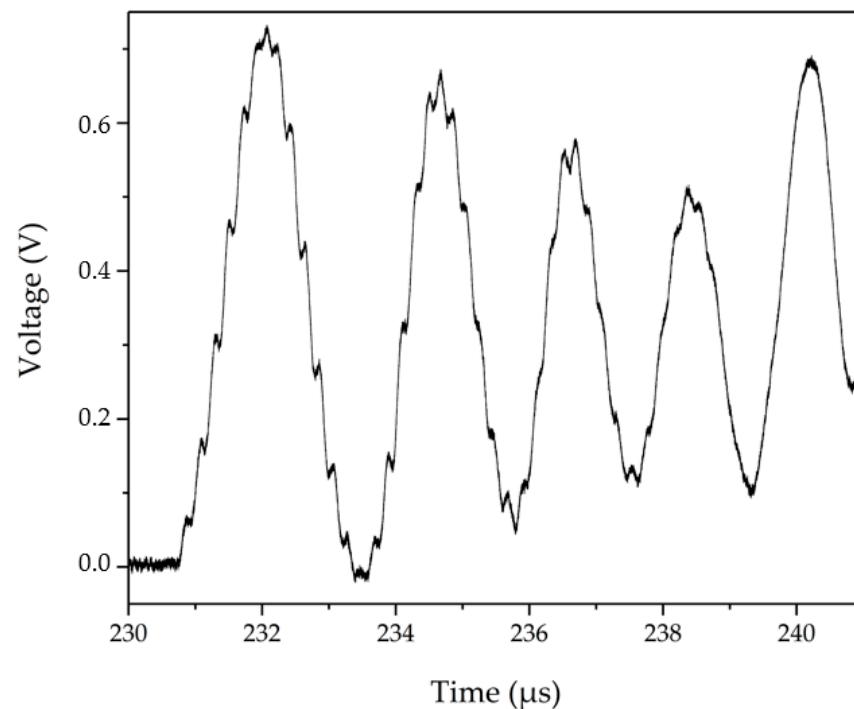


Figure 2. Typical waveform delivered by a 94 GHz interferometer during impact experiment on a TriAminoTrinitroBenzene (TATB) material (refractive index N_1 is of 1.78). The derivation of Doppler frequencies from the fitting process gives the following estimation: $N_2 = 2.37$ (shocked medium refractive index), $V_1 = 3850 \text{ m}\cdot\text{s}^{-1}$ (shock wavefront velocity) and $V_2 = 385 \text{ m}\cdot\text{s}^{-1}$ (particle velocity).

The manuscript is organized as follows. Section 2 briefly describes the previously reported method used to derive the shock wavefront and particle velocities from the estimation of two Doppler Frequencies, and discusses the limitations of this method. Section 3 describes the development of a new method based on Convolutional Neural Networks to overcome the limitations of the previously reported method. In Section 4, the performances of the two methods are compared for the derivation of the shock wavefront and particle velocities from the same set of measured waveforms.

2. Shock Wavefront and Particle Velocities Derived from Doppler Frequencies

The shock wavefront in a dielectric material is usually modeled by a moving interface (see, e.g., [21]), which separates the material in two dielectric regions; the region in front of the interface is called the *pristine medium* with a refractive index N_1 , while the region behind the interface is called the *shocked medium* with a refractive index N_2 . The incident electromagnetic field is then subjected to the reflection by and transmission through the dielectric interface with a Doppler frequency shift. In addition, the electromagnetic field encounters losses in the material. Two configurations are analyzed throughout the paper, the single and double interface configurations.

In the so-called *single interface configuration*, the dielectric interface models the shock wavefront. It moves toward a millimeter-wave interferometer, and the velocity V_1 of the interface is derived from the extraction of the Doppler frequency shift in the waveform delivered by the interferometer. The extraction requires the prior knowledge of pristine medium refractive index N_1 . The single interface configuration offers an exact solution for the waveform [8], which is used here to investigate the eventual benefits of the Neural Network approach for estimating the shock wavefront velocity V_1 .

The *double interface configuration* takes into account the metallic impactor or the transfer plate. Therefore, in addition to the reflection by the (E_R) and the transmission through the shock wave interface (E_T), the electromagnetic field transmitted by the interferometer experiences the reflection by and transmission through the moving interface between the

shocked medium and the metallic plate (see Figure 3). In this study, the metallic plate is assumed to be perfectly conductive, and consequently, the total electromagnetic reflection occurs at its surface, called E_{RC} . Following [8], both the velocity V_1 of the shock wavefront and the velocity V_2 of the metallic interface between the impactor (metallic plate) and the shocked medium may be derived from the measurement of two Doppler frequencies in the reflected electric field $E_R = E_{R1} + E_{R2} + E_{R3} + \dots$.

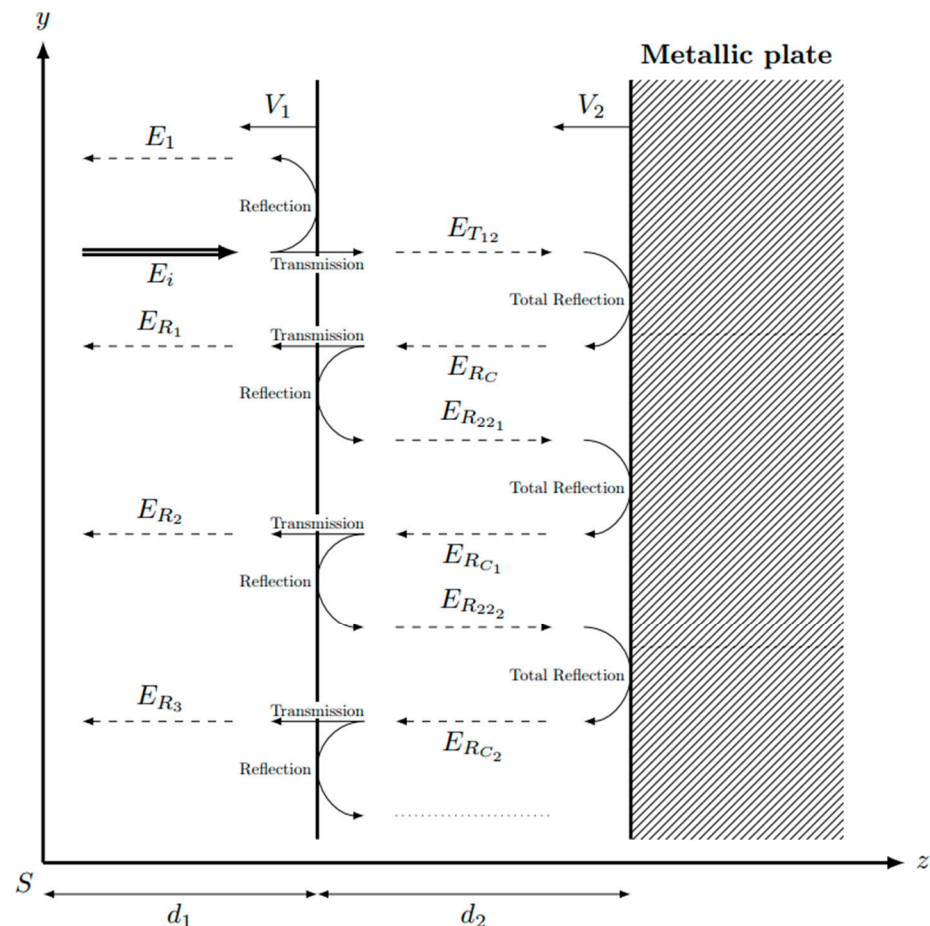


Figure 3. Scheme of the double interface configuration. The incident electric field E_i is normal to the shock wavefront, that is, the moving interface between the pristine material and shocked medium, with E_1 , first reflection; E_{Ri} , following transmission/reflection/transmission; E_T , first transmission; E_{RCi} , reflections on the metallic plate. The pristine material thickness is d_1 . The shocked medium thickness is d_2 .

As illustrated in Figure 2, typical measured waveforms actually exhibit two oscillations, whose frequency and magnitude are used here to estimate the velocities V_1 and V_2 (it is assumed here that the refractive index N_1 of the studied pristine material is known). This estimation may be performed from a fitting process which approximates the waveform by the linear combination $s(t)$ of two sine functions given by the following:

$$s(t) = A_1 \cdot \sin(2\pi f_1 \cdot t + \varphi_1) + A_2 \cdot \sin(2\pi f_2 \cdot t + \varphi_2) \quad (2)$$

where the fitting parameters are f_1 and f_2 (i.e., the unknown Doppler frequencies), A_1 , A_2 , φ_1 and φ_2 . We have observed that, for waveforms of sufficiently long duration ($>5 \mu\text{s}$), the fitting process allows for the detection of the two Doppler frequencies of interest, but as the waveform duration decreases, the accuracy of the lowest frequency estimation degrades gradually, and as a result, velocities V_1 and V_2 cannot be estimated precisely.

3. Shock Wavefront and Particle Velocities Derived from CNN Approach

The proposed approach requires the careful selection of the triplets (V_1 , V_2 , N_2) that are used in the simplified electromagnetic model of moving dielectric interface(s) reported in [8] for computing the waveforms and training the CNN.

An Artificial Neural Network (NN) with Multi-Layer Perceptron (MLP) [14] is an assembly of layers, each composed of several neurons, or nodes. As a biological neuron, each neuron linearly combines the outputs of the previous layer and applies an activation function to obtain the output. This function is often non-linear. Once the architecture of the NN is chosen, the learning process is launched. This stage consists of adjusting the parameters of each node to fit on a combination of inputs and outputs of the network. Here, the input is the N samples of the time-domain waveform delivered by the millimeter-wave interferometer during an impact experiment on dielectric materials, and the single output is the velocity V_1 of the shock wavefront, or the particle velocity V_2 , or else the refractive index N_2 of the shocked medium. Figure 4 shows an example of such NN. It consists of three layers; the first layer has five inputs and one bias, the second layer has three neurons and one bias and the third layer is composed of one output neuron which provides the estimation of the quantity of interest (that is, V_1 , V_2 or N_2). The bias is used to influence the output without interfering with the weights and the inputs. In the second layer, the output of each node is computed as follows using relation (3).

$$\text{Output} = f(w_1 \times \text{Input}_1 + w_2 \times \text{Input}_2 + w_3 \times \text{Input}_3 + w_4 \times \text{Input}_4 + w_5 \times \text{Input}_5 + w_b \times b) \quad (3)$$

where f is the scoring function, b denotes the bias, w_b designates the weight of the bias, Input_i are the inputs i and w_i is the weight of Input_i .

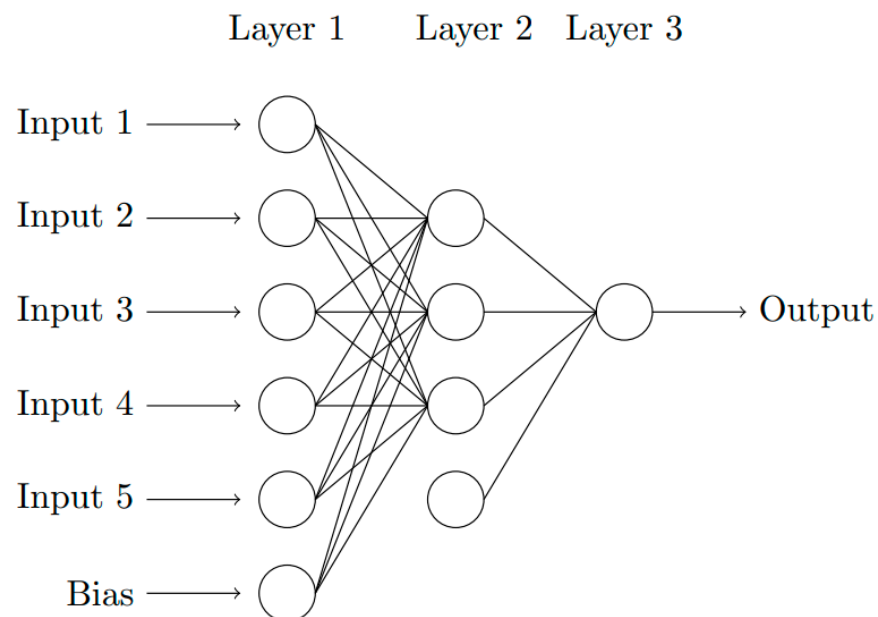


Figure 4. Simple architecture of a Neural Network (The circles represent the nodes).

In our investigation, the measurement data used in the input layer of the NN are annotated, i.e., they are known before they are processed in the NN. This case is also known as “supervised learning”, which is generally used to sort two types of problems as follows:

- Regression problems, where the problem is to estimate a quantity variable (V_1 , V_2 or N_2 in our study);
- Classification problems, where the problem is to predict a qualitative variable (i.e., a state, a category, etc.).

For any architecture, it would be possible here to process the waveform as a regression or classification problem, because it would either be possible to obtain the accurate value

of a velocity as output after the waveform processing, or to determine a range in which the velocity may be included. Anyway, for reasons of diagnostic accuracy, the analysis of waveforms will be considered here as a regression problem.

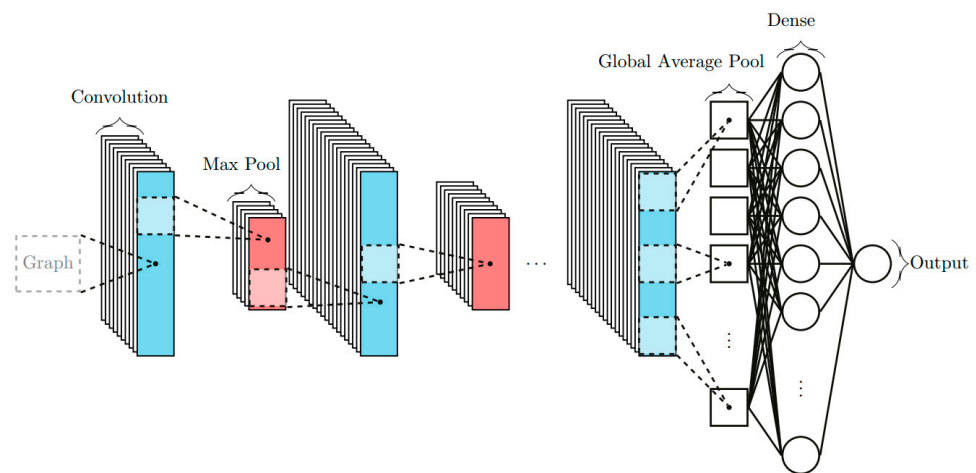
In view of the state-of-the-art (see, e.g., [15,16]), a fully connected dense model—i.e., each neuron in a layer receives an input from all the neurons of the previous layer—can accurately estimate the spectral content of some waveforms. The major drawback of this model is that the number of input neurons is fixed, and consequently, the same NN cannot process the variable number of waveform samples. Another limitation is that NN-based spectral analysis is not automated, so the signal processing is applicable to specific waveforms. Therefore, a fully connected dense model is not suitable to solve our inverse problem, either from using regression or classification methods. Another approach, based on a Convolutional Neural Network (CNN), is implemented here for the two configurations described in Section 2. The following is a well-known technique in raw signal processing [18,19]: The convolutional layers are filters that extract patterns from the signal; then, these patterns are processed by the dense layers to fit the output. The CNN is implemented here using Python 3.7.6 with the module Keras 2.8.0 [22] and the backend TensorFlow 2.9.3 [23]. The number of convolutional and dense layers is computed by fitting various architectures on the validation waveform data. The architecture of the network is identical for the following two configurations:

- In the *single medium configuration*, two networks are studied; the first network has the shock wavefront velocity V_1 as single output and the second has only the refractive index N_2 of the shocked medium as output;
- For the *double medium configuration*, three networks are studied; the first network has the shock wavefront velocity V_1 as output, the second one has the particle velocity V_2 and the third one has the refractive index N_2 of the shocked medium.

The waveform samples are normalized from a Glorot normal initialization [24]. This approach was found to be more efficient than a single CNN with two or three outputs. The inputs for the networks are the refractive index N_1 of the pristine material, the operating frequency (94 GHz) of the millimeter-wave interferometer, the time step used for the sampling of waveforms and the samples of waveforms delivered by the interferometer. The first architecture was made with a 16-layer neural network, inspired by the A.Dore Thesis [25,26]. Then, the architecture was enlarged to 18 layers in order to improve the precision and the generalization prediction. For this publication, the train set is 246,000 samples, the validation set is 30,000 samples and the test set is also 30,000 samples. For the comparisons between the DFA and NNA, the number of samples is 1000 for the single medium configuration and for the double medium configuration. The final network has four convolutional layers and seven dense layers (see Table 1). The convolutional layers perform the filtering operation, while the dense layers create linear combinations with bias. The maximum pooling layer selects the maximum value in a range of neurons. Batch normalization is a well-known technique in neural networks to overcome overfitting, which may occur when the algorithm performs well on training data but performs badly on any other data. This regularization technique allows the algorithm to keep its generalization ability [27]. The global average pooling layer makes the average in the selected range and flattens the filters from the previous convolutional layer to decrease the data size for the next layer, and consequently, to reduce the calculation time without interfering with the training process. Figure 5 sketches the action of every layer.

Table 1. Final CNN for each parameter V_1 , V_2 and N_2 as output.

Index of Layer	Type of Layer	Keras Name	Activation Function	Properties
1	Convolution	Conv1D	Rectified Linear Unit (ReLU)	72 filters, length 10
2	Normalization	BatchNormalization		
3	Convolution	Conv1D	ReLU	144 filters, length 10
4	Normalization	BatchNormalization		
5	Pooling	MaxPooling1D		
6	Convolution	Conv1D	ReLU	288 filters, length 10
7	Normalization	BatchNormalization		
8	Pooling	MaxPooling1D		
9	Convolution	Conv1D	ReLU	576 filters, length 10
10	Normalization	BatchNormalization		
11	Pooling	GlobalAveragePooling1D		
12	Dense	Dense	ReLU	50 neurons
13	Dense	Dense	tanh	60 neurons
14	Dense	Dense	tanh	40 neurons
15	Dense	Dense	tanh	30 neurons
16	Dense	Dense	ReLU	20 neurons
17	Dense	Dense	tanh	10 neurons
18	Dense	Dense	hard sigmoid	1 neuron

**Figure 5.** Scheme of the CNN used for determining the shock wavefront V_1 , the particle velocity V_2 or the refractive index N_2 of the shocked medium from waveforms delivered by the 94 GHz millimeter-wave interferometer.

The learning process is performed from the simulated waveforms provided by the electromagnetic model developed in [8]. The model is applied to create waveforms with multiple initial parameters. It allows using larger networks and prevents overfitting, which may occur when a limited number of experimental data is available. Moreover, the main advantage of using simulated inputs for the CNN training is that we can generate a large data set which makes possible the derivation of the accurate estimation of velocities or refractive index. The main idea is that the waveform is composed of two main contributions. The first is the electric field directly reflected by the shock wavefront. The second contribution combines multiple reflections of the electric field inside the dielectric sample. For each of contributions, the reflection and transmission coefficients are computed. The adequate

number of reflections in the shocked medium (see Figure 3) is derived from the numerical convergence of the total reflected electric field. Table 2 reports the mean difference between the computed waveforms. The chosen number of reflections in the shocked medium is set to four, as the difference with the waveform with five internal reflections does not exceed 0.004%. The learning process is performed with the Adam optimizer with the coefficients given in [28] and with a mean squared error loss. The maximum number of full training cycles or *epochs* is set to 200. However, the learning rate decreases if the loss is constant over five epochs. In practice, the maximum number was never reached, as the loss converged rapidly. To ensure that the loss is not on a plateau, ten more epochs are computed after reaching numerical convergence. To avoid overfitting, new validation data are computed at each epoch.

Table 2. Mean difference of the total reflection between signals for different number of internal reflections in the shocked dielectric sample.

Number of Considered Reflections in the Shocked Medium	Total Reflection Mean Difference (%)
1 and 2	5.7
2 and 3	0.5
3 and 4	0.05
4 and 5	0.004
5 and 6	0.0004

The refractive index of both the pristine material and the shocked material, denoted, respectively, by N_1 and N_2 , and the velocity V_1 of the shock wavefront and the particle velocities V_2 are randomly generated for each waveform. The time duration of waveforms is also randomly modified to account for various experimental conditions. The quantities of interest are normalized before the validation step during the learning phase. The boundaries for each parameter are listed in Table 3. These bounds are chosen to be representative of the experimental values. Following [29], the refractive index of the dielectric material increases when submitted to a shock wave. Therefore, during the learning stage, N_2 is computed as the summation of N_1 with a random number ranging from 0 to 1. All the signals for the train set, the validation set and the test set are generated with the Table 3 parameter ranges (N_1 , N_2 , V_1 , V_2 , measurement duration). Thus, V_1 , V_2 and N_2 are the initial parameters chosen to determine the frequencies and the amplitude values and are therefore directly known and correlated to these values. So, it is very helpful for the uncertainty analysis, because the pristine values (V_1 , V_2 , and N_2) are compared directly to the retrieved ones using the DFA or NNA method. Therefore, the frequencies and the amplitudes are intermediate values. Especially for the DFA, they are the output of the double sinus method, and the associated V_1 , V_2 and N_2 are calculated back with the physical model using Equations (35)–(37) in reference [8].

Table 3. Parameters boundaries for the learning step of the CNN.

Parameter	Minimum Value	Maximum Value
Material at rest refractive index N_1	1	2
Shocked material refractive index N_2	1	3
Particle velocity V_2 (m s^{-1})	300	500
Shock wavefront velocity V_1 (m s^{-1})	3000	5000
Measurement duration (μs)	2	3.5

4. Results and Discussion

4.1. Single Medium Configuration

To compare the performances of the two methods reported in Sections 2 and 3, that is, the technique based on the extraction Doppler frequencies [8] (DFA, which stands for Doppler Frequency Approach) and the proposed Neural Network Approach (NNA), one thousand random waveforms with a length of 10,000 points based on the Table 3 ranges are computed and processed. With the chosen CNN, the output values are obtained from the predict method from the Keras 2.8.0 module [22]. As the fitting process is direct, the value is simply calculated by the Fast Fourier Transform and directly compared with the outputs of the CNN. The procedure is sketched in Figure 6. The number of samples versus the relative prediction error are presented in Figure 7 on V_1 and N_2 for the NNA and DFA. The error displayed on the graph abscissa is the difference between the values used to generate the signal and the values predicted by the NNA or DFA after the analysis of this same signal. No difference is obtained between the DFA and NNA for the single medium configuration. For the shock wavefront velocity V_1 and the refractive index N_2 of the shocked medium, the two methods provide similar results and accuracy. Following these encouraging results, the neural network is applied in Section 4.2 to the double medium configuration, which consists of a much more realistic model for the practical situation.

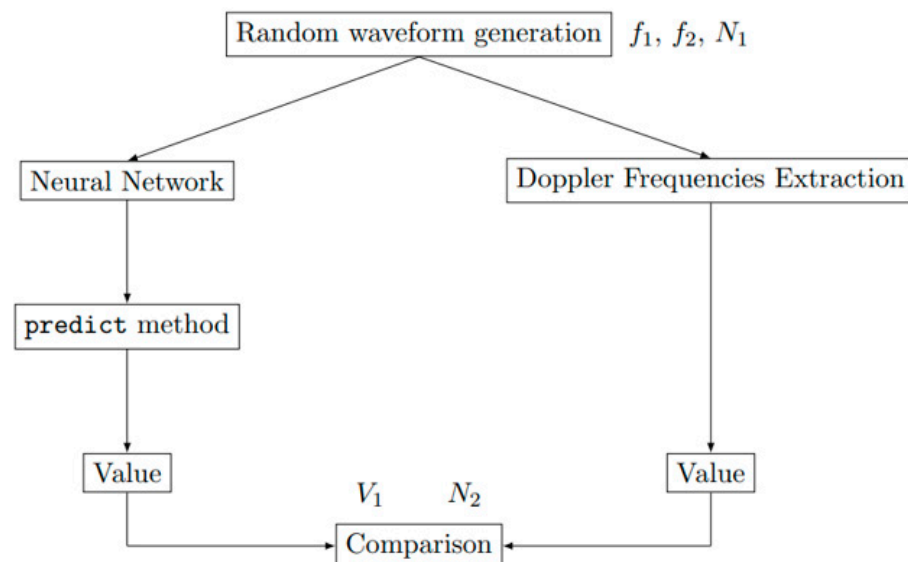


Figure 6. Sketch for the comparison of the Neural Network Approach (see Section 3) and the Doppler Frequency Approach (see Section 2) applied to the single medium configuration.

4.2. Double Medium Configuration

For the double medium configuration, one thousand random waveforms with a length of 10,000 points based on the Table 3 ranges are computed from the electromagnetic model reported in [8] and are used for training the CNN. As in Section 4.1, the output values are obtained by using the predict method from the Keras 2.8.0 module. For deriving the velocity V_1 or V_2 from the DFA, the resolution is not straightforward; as the number of comparison points increases, the fitting process using two sine functions (see Section 2) must be performed automatically by using an initial guess vector for the parameters. The fitted waveform is computed and correlated with the input waveform. Let the correlation coefficient $\rho_{X,Y}$ of two investigated waveforms X and Y be defined as follows:

$$\rho_{X,Y} = \frac{cov(X,Y)}{\sigma_X \sigma_Y} \quad (4)$$

where cov denotes the co-variance operator, while σ_X and σ_Y designate the standard deviation of X and Y . If $\rho_{X,Y}$ is smaller than a prescribed threshold, the input waveform is

discarded because the fitting process is considered to be unsuccessful. This method is repeated until 1000 waveform samples with a length of 10,000 points have been obtained. Two examples of computed waveforms are plotted in Figure 8, as well as the result of the DFA and corresponding correlation coefficients. The procedure is sketched in Figure 9. For comparison purposes, we determine the difference between V_1 , V_2 and N_2 estimated from the DFA and NNA, with the exact values selected for the waveform computation. The mean value M of the difference and the standard deviation for each method are reported in Table 4. A systematic error (i.e., the mean is not zero) is present for both methods, but it is smaller for the NNA than for the DFA. The NNA also yields a smaller standard deviation than the DFA. As expected, the higher the correlation coefficient $\rho_{X,Y}$ (or equivalently, the more accurate the derivation of Doppler frequencies and magnitudes), the more accurate the estimation of V_1 , V_2 and N_2 provided by the DFA. However, as the correlation coefficient increases, the systematic error on the estimation of V_1 , V_2 and N_2 provided by the NNA is constant, even for short-duration waveforms. The number of samples versus the relative prediction error are presented in Figure 10 for the DFA and NNA. These distributions are displayed for three different correlation coefficients, 0.9, 0.99 and 0.999. The relative prediction error is the difference between the predicted values and the true values of V_1 , V_2 and N_2 . Table 4 is the analyzed table of Figure 10. The mean value and the standard deviation for CNN are, respectively, less than 1.1% and 11.4% for the parameter V_1 . The mean value and the standard deviation for CNN are, respectively, less than 1.6% and 9.4% for the parameter V_2 . The mean value and the standard deviation for CNN are, respectively, less than 0.1% and 0.1% for the parameter N_2 . So, compared to the DFA in Table 4 and Figure 10, the mean values of the NNA test set are near zero, showing a more precise method as a centered distribution, and the standard deviations of the NNA test set are reduced, showing less dispersed values. For the very large correlation coefficient, the methods of the NNA and DFA are quite similar. This seems logical, because the DFA is more precise in this case. However, we continue to observe large deviations for the DFA method. As typical experimental values for the correlation coefficient are between 0.9 and 0.99 [10], the NNA should then be preferred when processing short-duration waveforms, especially for estimating the particle velocity V_2 and refractive index N_2 of the shocked medium.

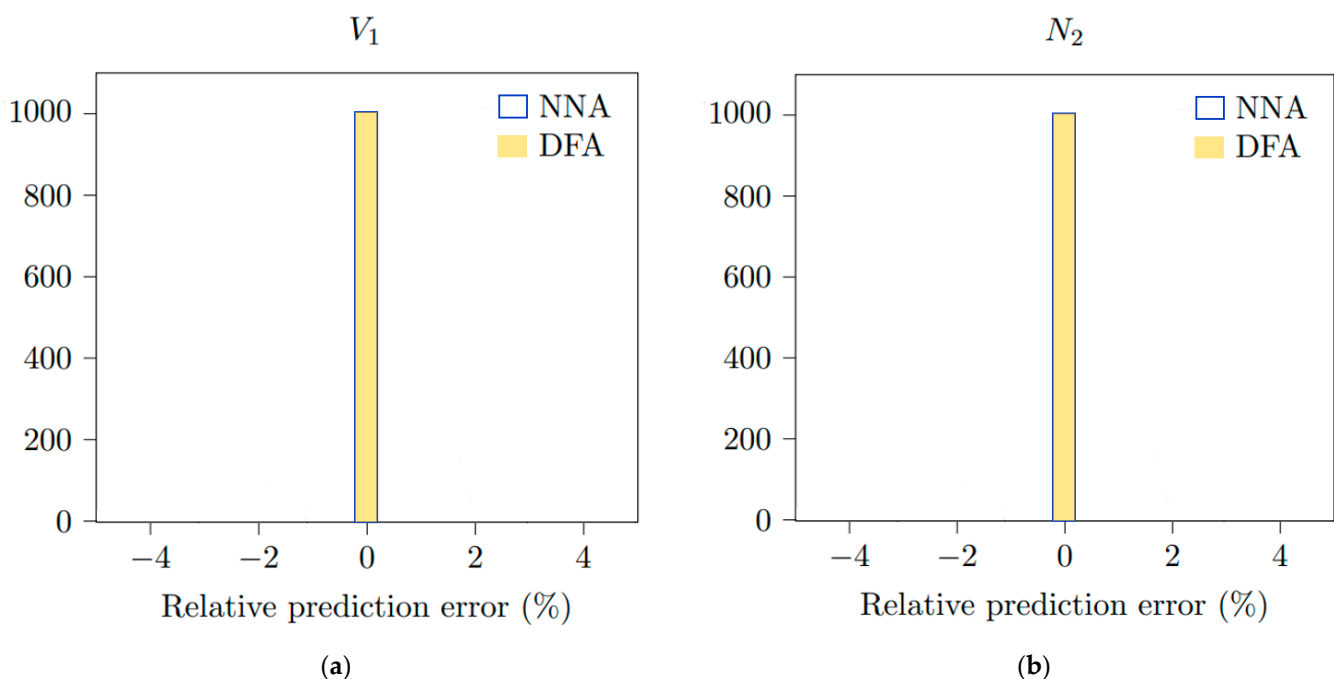


Figure 7. (a) Relative prediction error distribution on V_1 derived from NNA and DF, and (b) relative prediction error distribution on N_2 determined from NNA and DF (single medium configuration). The number of comparison samples is 1000.

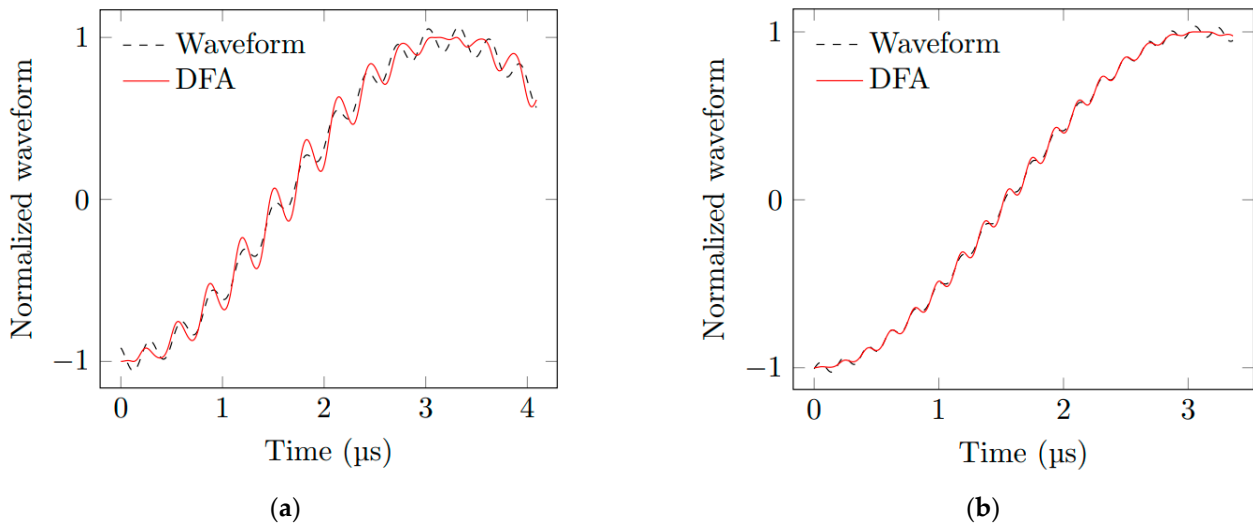


Figure 8. Dimensionless waveforms computed with $V_1 = 4000 \text{ m s}^{-1}$, $V_2 = 400 \text{ m s}^{-1}$ and $N_2 = 2$ (dashed line), and the waveforms derived from the DFA fitting process (in red line) for various correlation coefficients, (a) $\rho_{X,Y} = 0.997$ and (b) $\rho_{X,Y} = 0.9998$.

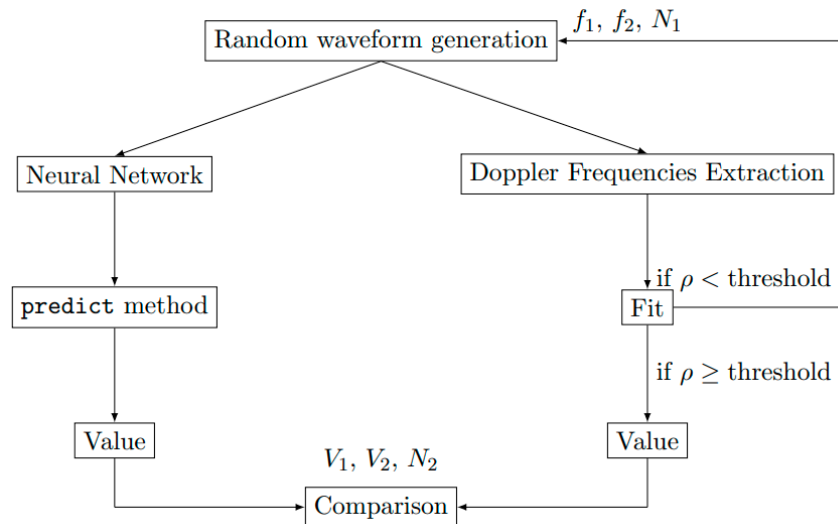


Figure 9. Sketch for the comparison of the Neural Network Approach (see Section 3) and the Doppler Frequency Approach (see Section 2) applied to the double medium configuration.

Table 4. Mean and standard deviation of the difference between V_1 , V_2 and N_2 estimated from DFA and NNA, with the exact values selected for the waveform computation.

Method Name	V_1		V_2		N_2		$\rho_{X,Y}$
	M (%)	σ (%)	M (%)	σ (%)	M (%)	σ (%)	
Neural Network Approach	-0.1	9.8	0.6	9.4	-0.1	-0.1	0.9
Doppler Frequency Approach	-5.9	38.1	37.9	115.2	1.4	1.4	
Neural Network Approach	-1.1	10.0	0.1	9.2	-0.1	-0.1	0.99
Doppler Frequency Approach	-9.6	29.8	32.2	100.7	7.0	7.0	
Neural Network Approach	-1.0	11.4	-1.6	9.3	0.0	0.0	0.999
Doppler Frequency Approach	-7.6	33.3	-6.5	35.9	2.6	2.6	

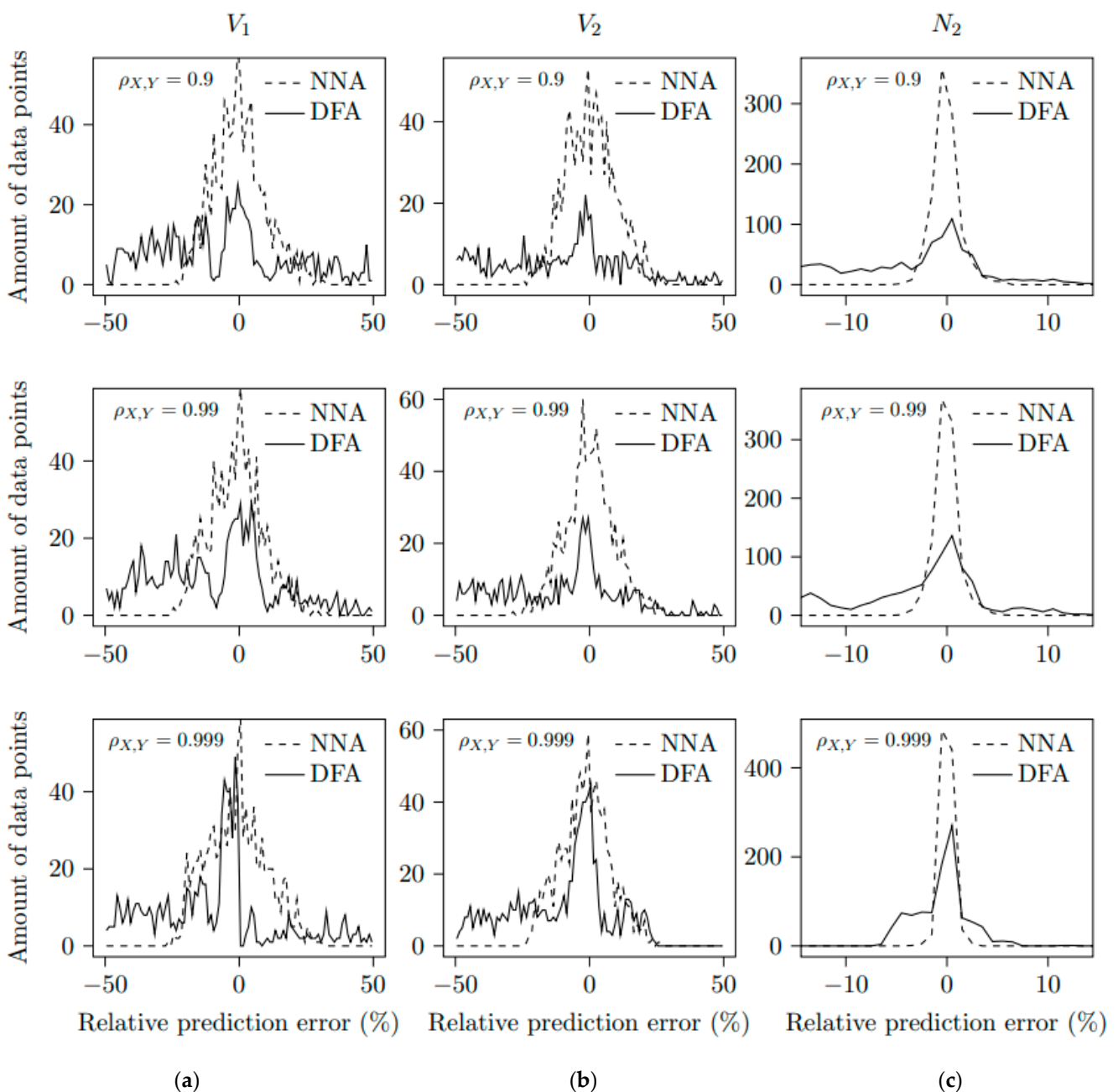


Figure 10. Relative prediction error distribution given by NNA and DFA with thresholds $\rho_{X,Y} = 0.9$ (up), 0.99 (middle) and 0.999 (down) for determination of (a) the shock wavefront velocity V_1 , (b) particle velocity V_2 and (c) the refraction index N_2 of the shocked medium.

5. Conclusions

In this paper, a convolutional neural network is proposed for solving an electromagnetic inverse problem involving solid dielectric materials subjected to mechanical impacts. From the computed waveforms delivered by a millimeter-wave interferometer, the convolutional network provides more accurate estimations of the shock wavefront velocity in the shocked materials, the particle velocity, as well as the refractive index of the shocked medium, for short-duration waveforms of a few microseconds less than a time period long, compared to the Doppler Frequency Analysis, based on the fitting parameters of the sum of two sine functions. These results significantly extend the application of millimeter-wave interferometry to the investigation of dielectric materials subjected to steady shocks.

Work is ongoing to improve the network architecture in order to reduce the standard error prediction for each parameter.

Author Contributions: Conceptualization, H.A., A.L., M.L. and Y.B.; methodology, A.D., B.R. and J.M.; software, B.R., J.M. and S.C.; validation, H.A., A.D. and S.C.; formal analysis, J.M. and B.R.; investigation, J.M. and B.R.; resources, A.L. and H.A.; data curation, J.M., B.R. and S.C.; writing—original draft preparation, J.M. and B.R.; writing—review and editing, A.L., J.M. and H.A.; visualization, M.L. and Y.B.; supervision, H.A., A.L., M.L. and Y.B.; project administration, A.L. and H.A.; funding acquisition, A.L. All authors have read and agreed to the published version of the manuscript.

Funding: This work was funded by the French Procurement Agency DGA under research fundings.

Institutional Review Board Statement: Not applicable.

Informed Consent Statement: Not applicable.

Data Availability Statement: The data presented in this study are available on request from the corresponding author.

Acknowledgments: The work and improvements on the convolutional neuronal network were carried out within the LRC LICUR framework.

Conflicts of Interest: The authors declare no conflict of interest.

References

1. Meyers, M.A. *Dynamic Behavior of Materials*; John Wiley and Sons: Berkeley, CA, USA, 1994.
2. Marsh, S.P. *Dynamic Behavior of Materials*; University of California Press: New York, NY, USA, 1980.
3. Forbes, J.W. *Shock Wave Compression of Condensed Matter*; Springer: Berlin/Heidelberg, Germany, 2012.
4. Bel'skii, V.M.; Mikhailov, A.L.; Rodionov, A.V.; Sedov, A.A. Microwave Diagnostics of Shock-Wave and Detonation Processes. *Combust. Explos. Shock Waves* **2011**, *47*, 639–650. [[CrossRef](#)]
5. Mitchell, A.C.; Nellis, W.J. Shock compression of aluminum, copper, and tantalum. *J. Appl. Phys.* **1981**, *52*, 3363. [[CrossRef](#)]
6. Cranch, G.A.; Lunsford, R.; Grn, J.; Weaver, J.; Compton, S.; May, M.; Kostinski, N. Characterization of laser-driven shock waves in solids using a fiber optic pressure probe. *Appl. Opt.* **2013**, *52*, 7791–7796. [[CrossRef](#)] [[PubMed](#)]
7. Poef, S.; Genetier, M.; Lefrancois, A.; Osmont, A.; Baudin, G.; Chinnayya, A. Investigation of JWL Equation of State for Detonation Products at Low Pressure with Radio Interferometry. *Propellants Explos. Pyrotech.* **2018**, *43*, 1157. [[CrossRef](#)]
8. Rougier, B.; Aubert, H.; Lefrancois, A.; Barbarin, Y.; Luc, J.; Osmont, A. Reflection of Electromagnetic Waves From Moving Interfaces for Analyzing Shock Phenomenon in Solids. *Radio Sci.* **2018**, *53*, 888–894. [[CrossRef](#)]
9. Rougier, B.; Aubert, H.; Lefrancois, A. Measurement of Shock Wave and Particle Velocities in Shocked Dielectric Material from Millimeter-Wave Remote Sensing. In Proceedings of the 2018 48th European Microwave Conference (EuMC), Madrid, Spain, 23–27 September 2018.
10. Rougier, B.; Lefrancois, A.; Aubert, H.; Bouton, E.; Luc, J.; Osmont, A.; Barbarin, Y. Simultaneous Shock and Particle Velocities Measurement using a Single Microwave Interferometer on Pressed TATB Composition T2 Submitted to Plate Impact. In Proceedings of the International Detonation Symposium, Cambridge, MD, USA, 15–20 July 2018.
11. Krall, A.D.; Glancy, B.C.; Sandusky, H.W. Microwave interferometry of shock waves. I. unreacting porous media. *J. Appl. Phys.* **1993**, *74*, 6322–6327. [[CrossRef](#)]
12. Hawke, R.S.; Keeler, R.N.; Mitchell, A.C. Microwave dielectric constant of Al₂O₃ at 375 kilobars. *Appl. Phys. Lett.* **1969**, *14*, 229–231. [[CrossRef](#)]
13. Kanakov, V.A.; Lupov, S.Y.; Orekhov, Y.I.; Rodionov, A.V. Techniques for retrieval of the boundary displacement data in gas-dynamic experiments using millimeter-waveband radio interferometers. *Radiophys. Ans Quantum Electron.* **2008**, *51*, 210–221. [[CrossRef](#)]
14. Zhang, Q.J.; Gupta, K.C.; Devabhaktuni, V.K. Artificial neural networks for RF and microwave design—from theory to practice. *IEEE Trans. Microw. Theory Tech.* **2003**, *51*, 1339–1350. [[CrossRef](#)]
15. Hornik, K. Approximation capabilities of multilayer feedforward networks. *Neural Netw.* **1991**, *4*, 251–257. [[CrossRef](#)]
16. Noel, S.E.; Szu, H.H.; Gohel, Y.J. Doppler frequency estimation with wavelet and neural networks. *Wavelet Appl. V* **1998**, *3391*, 150–158.
17. Verma, P.; Schafer, R.W. Frequency Estimation from Waveforms using Multi-Layered Neural Networks. In Proceedings of the Interspeech, San Francisco, CA, USA, 8–12 September 2016; pp. 2165–2169.
18. Palaz, D.; Magamai.-Doss, M.; Collobert, R. Analysis of CNN-based speech recognition system using raw speech as input. In Proceedings of the Interspeech, Dresden, Germany, 6–10 September 2015; pp. 11–15. [[CrossRef](#)]
19. Fan, R.; Liu, G. CNN-Based Audio Front End Processing on Speech Recognition. In Proceedings of the 2018 International Conference on Audio, Language and Image Processing (ICALIP), Shanghai, China, 16–17 July 2018; pp. 349–354.
20. Lecun, Y.; Bengio, Y. Convolutional networks for images, speech, and time series. *Handb. Brain Theory Neural Netw.* **1995**, *3361*, 10.

21. Sivakumar, A.; Suresh, S.; Anto Pradeep, J.; Balachandar, S.; Martin Britto Dhas, S.A. Effect of Shock Waves on Dielectric Properties of KDP Crystal. *J. Electron. Mater.* **2018**, *47*, 4831–4839. [[CrossRef](#)]
22. Chollet, F. and Others. Keras. 2015. Available online: <https://keras.io> (accessed on 8 March 2023).
23. Abadi, M.; Agarwal, A.; Barham, P.; Brevdo, E.; Chen, Z.; Citro, C.; Corrado, G.S.; Davis, A.; Dean, J.; Devin, M.; et al. TensorFlow: Large-Scale Machine Learning on Heterogeneous Systems. *arXiv* **2016**, arXiv:1603.04467.
24. Glorot, X.; Bengio, Y. Understanding the difficulty of training deep feedforward neural networks. In Proceedings of the Thirteenth International Conference on Artificial Intelligence and Statistics, Sardinia, Italy, 13–15 May 2010; pp. 249–256.
25. Dore, A. Suivi Individualisé du Déplacement D’insectes Pollinisateurs et D’animaux D’élevage à L’aide de RADARs Microondes à Modulation de Fréquence. Ph.D. Thesis, Université Toulouse 2—Jean-Jaurès, Laboratoire LAAS-CNRS, Toulouse, France, 2021. Available online: https://oatao.univ-toulouse.fr/28462/1/Dore_alexandre.pdf (accessed on 8 March 2023).
26. Zhang, X.; Zou, J.; He, K.; Sun, J. Accelerating very deep convolutional networks for classification and detection. *IEEE Trans. Pattern Anal. Mach. Intell.* **2015**, *38*, 1943–1955. [[CrossRef](#)] [[PubMed](#)]
27. Ioffe, S.; Szegedy, C. Batch Normalization: Accelerating Deep Network Training by Reducing Internal Covariate Shift. *arXiv* **2015**, arXiv:1502.03167.
28. Kingma, D.; Ba, J. Adam: A Method for Stochastic Optimization. *arXiv* **2014**, arXiv:1412.6980.
29. Davison, L.; Graham, R.A. Shock compression of solids. *Phys. Rep.* **1979**, *55*, 255–379. [[CrossRef](#)]

Disclaimer/Publisher’s Note: The statements, opinions and data contained in all publications are solely those of the individual author(s) and contributor(s) and not of MDPI and/or the editor(s). MDPI and/or the editor(s) disclaim responsibility for any injury to people or property resulting from any ideas, methods, instructions or products referred to in the content.